NASA/TM-2008-215530

Fracture Testing of Integral Stiffened Structure

John A. Newman, Stephen W. Smith, and Robert S. Piascik
Langley Research Center, Hampton, Virginia

David S. Dawicke
Analytical Services and Materials, Inc., Hampton, Virginia

William M. Johnston and Scott A. Willard
Lockheed Martin Engineering and Sciences
Langley Research Center, Hampton, Virginia

October 2008

The NASA STI Program Office . . . in Profile

Since its founding, NASA has been dedicated to the advancement of aeronautics and space science. The NASA Scientific and Technical Information (STI) Program Office plays a key part in helping NASA maintain this important role.

The NASA STI Program Office is operated by Langley Research Center, the lead center for NASA's scientific and technical information. The NASA STI Program Office provides access to the NASA STI Database, the largest collection of aeronautical and space science STI in the world. The Program Office is also NASA's institutional mechanism for disseminating the results of its research and development activities. These results are published by NASA in the NASA STI Report Series, which includes the following report types:

- TECHNICAL PUBLICATION. Reports of completed research or a major significant phase of research that present the results of NASA programs and include extensive data or theoretical analysis. Includes compilations of significant scientific and technical data and information deemed to be of continuing reference value. NASA counterpart of peer-reviewed formal professional papers, but having less stringent limitations on manuscript length and extent of graphic presentations.

- TECHNICAL MEMORANDUM. Scientific and technical findings that are preliminary or of specialized interest, e.g., quick release reports, working papers, and bibliographies that contain minimal annotation. Does not contain extensive analysis.

- CONTRACTOR REPORT. Scientific and technical findings by NASA-sponsored contractors and grantees.

- CONFERENCE PUBLICATION. Collected papers from scientific and technical conferences, symposia, seminars, or other meetings sponsored or co-sponsored by NASA.

- SPECIAL PUBLICATION. Scientific, technical, or historical information from NASA programs, projects, and missions, often concerned with subjects having substantial public interest.

- TECHNICAL TRANSLATION. English-language translations of foreign scientific and technical material pertinent to NASA's mission.

Specialized services that complement the STI Program Office's diverse offerings include creating custom thesauri, building customized databases, organizing and publishing research results ... even providing videos.

For more information about the NASA STI Program Office, see the following:

- Access the NASA STI Program Home Page at ***http://www.sti.nasa.gov***

- E-mail your question via the Internet to help@sti.nasa.gov

- Fax your question to the NASA STI Help Desk at (301) 621-0134

- Phone the NASA STI Help Desk at (301) 621-0390

- Write to:
  NASA STI Help Desk
  NASA Center for AeroSpace Information
  7115 Standard Drive
  Hanover, MD 21076-1320

NASA/TM-2008-215530

Fracture Testing of Integral Stiffened Structure

John A. Newman, Stephen W. Smith, and Robert S. Piascik
Langley Research Center, Hampton, Virginia

David S. Dawicke
Analytical Services and Materials, Inc., Hampton, Virginia

William M. Johnston and Scott A. Willard
Lockheed Martin Engineering and Sciences
Langley Research Center, Hampton, Virginia

National Aeronautics and
Space Administration

Langley Research Center
Hampton, Virginia 23681-2199

October 2008

Available from:

NASA Center for AeroSpace Information (CASI)
7115 Standard Drive
Hanover, MD 21076-1320
(301) 621-0390

National Technical Information Service (NTIS)
5285 Port Royal Road
Springfield, VA 22161-2171
(703) 605-6000

Abstract

Laboratory testing was conducted to evaluate safety concerns for integrally-stiffened tanks that were found to have developed cracks during pressurization testing. Cracks occurrred at fastener holes where additional stiffeners were attached to the intregrally-stiffened tank structure. Tests were conducted to obtain material properties and to reproduce the crack morphologies that were observed in service to help determine if the tanks are safe for operation. Reproducing the cracking modes observed during presurization testing required a complex loading state involving both a tensile load in the integrally-stiffenened structure and a pin-load at a fastener hole.

Introduction

Rocket fuel tanks were manufactured from aluminum alloy 2014 plate material to create integrally-stiffened tank walls consisting of four sections, each bent into a quarter-arc. Four pieces of integrally-stiffened plates were welded together to form a cylindrical tank. The structure was originally designed to accomodate five external solid rocket boosters. To increase vehicle performance, the use of seven solid rocket boosters was required for specific missions. To accommodate the increased stresses in the structure, tanks were modified from their original design such that multiple 7000-series aluminum alloy stiffeners were placed inside the tank and fastened to the isogrid ribs, also called integral stiffeners, as shown schematically in Figure 1. One of the tanks ruptured during pressurization testing of these modified integrally-stiffened tanks in 2005. Visual inspection revealed cracking in all but two of the remaining tanks and that cracks occurred in the region at the end of the stiffener, near the location that loads are transferred through isogrid nodes, as shown in Figure 1.

All of the cracks found emanated from the fastener hole at the end of the stiffener and cracked through the rib thickness, propagating towards the center of the tank. (See Figure 1.) (Note that the exterior surfaces of these fuel tanks are smooth and the isogrid ribs are contained within the tanks.) Generally, these cracks were normal (perpendicular) to the tank wall (labeled as primary crack in Figure 1). Some of these end holes also contained cracks that propagated towards the outer skin of the tank; however, these cracks grew at an angle of approximately 18^{o} to the tank (labeled as secondary crack #1 in Figure 1). Cracks running parallel to the tank wall emanating from the end fastener hole (nearest isogrid node) toward the next fastener hole were also observed in some tanks (See secondary crack #2 in Figure 1). Considering that all holes contained cracks growing towards the inside of the tank, it was believed that this cracking mode occurred first and, thus, these cracks were called “primary” cracks. Cracks growing towards the outer skin or from fastener hole to fastener hole of the tank were called “secondary” cracks. Although primary cracks are damaging and alter the local loading at the stiffener end, these cracks were considered to be less threatening than secondary cracks because they will not result in a breach of the outer tank skin, thereby, producing a leak.

The objective of this work is to reproduce the crack morphologies that occurred during the pressurization testing and determine the validity of the hypothesis that primary cracking occurs first either without secondary cracking or with relatively benign secondary cracking. Laboratory specimens were made of aluminum alloy 2014 plate material. While this material is nominally the same as the original material used to construct the tanks, material from the original lot would have been preferred, but was not available for study. Therefore, limited material properties testing was performed to evaluate the material used to fabricate specimens and to obtain the properties required for structural analysis.

A significant concern with the stiffened structure is that a row of fastener holes was machined into the isogrid ribs of the tank perpendicular to the thickness of the original plate product. This configuration creates high-stress regions in the isogrid rib acting along the weakest orientation (perpendicular to plate thickness) in plate materials. Any testing and analysis should consider the anisotropic nature of the tank material.

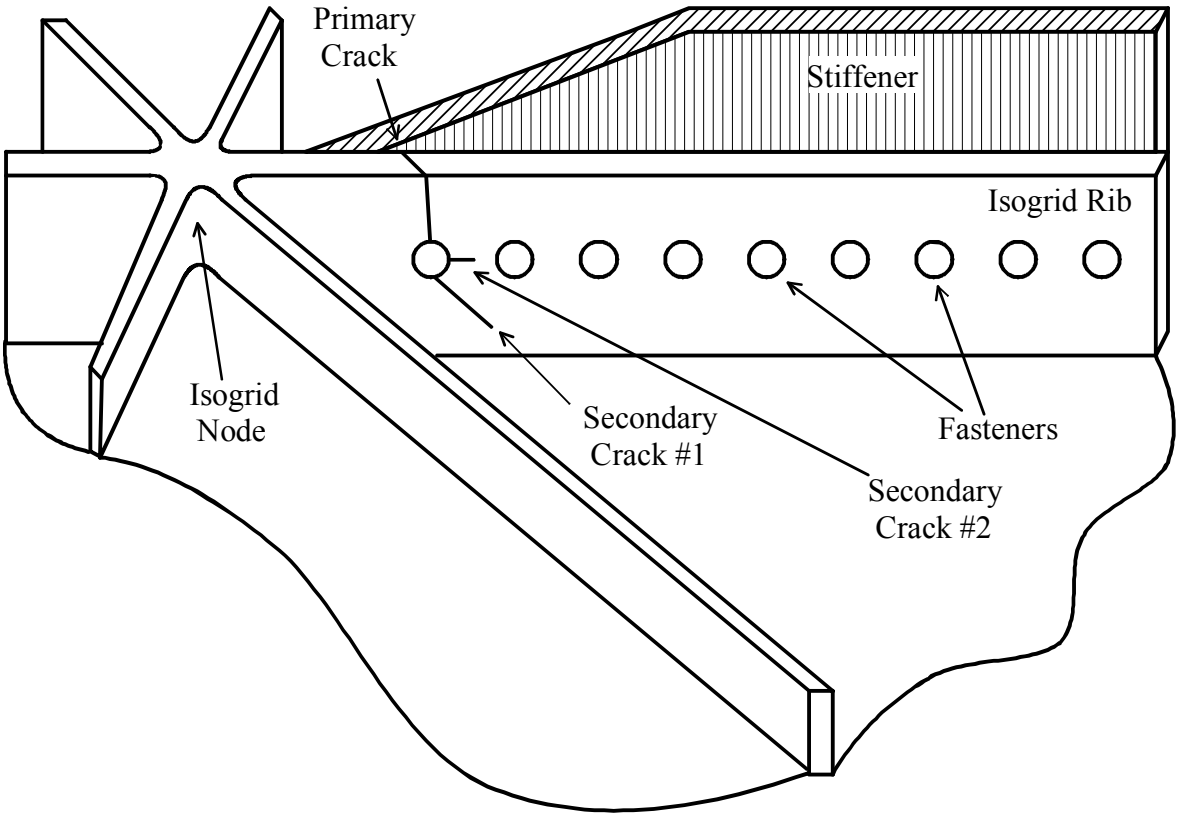

Figure 1. Configuration of primary and secondary cracks.

Approach

A series of tests were conducted to reproduce the crack configuration observed during tank pressurization. Specimens were machined from aluminum 2014 plate material to capture the geometric and anisotropic characteristics of the tank structure. A series of tensile tests and fracture toughness tests were conducted, in accordance with American Society for Testing and Materials (ASTM) standards, to determine the mechanical properties corresponding to primary and secondary cracking, with respect to plate orientations. Testing was also performed on specimens containing holes similar to the isogrid rib fastener holes to reproduce the crack configuration observed in service and to better understand how the anisotropic variation in material properties affects the cracking behavior. The tests performed on specimens containing holes are schematically illustrated in Figure 2.

The initial tests were performed on tensile specimens with a hole in the center of the gage section (see Figure 2a), and were intended to determine the effect of a hole on remote loading (not applied at the fastener). The second set of tests was conducted on a specimen containing two holes (see Figure 2b). The presence of multiple holes allows hole-to-hole secondary cracking (see secondary crack #2 in Figure

1), and, through the use of reaction blocks connected to the specimen through tight-fitting pins, allows load to be applied through the fastener holes. Finally, a third specimen (see Figure 2c) was designed to better simulate the local geometry, which possesses multiple fastener holes and outer tank skin. The third specimen design used a fixed stiffener bar to provide pin loading while testing under increasing axial and transverse displacement to achieve the complex combination of pin loading and remote loading that occurs in the tank structure.

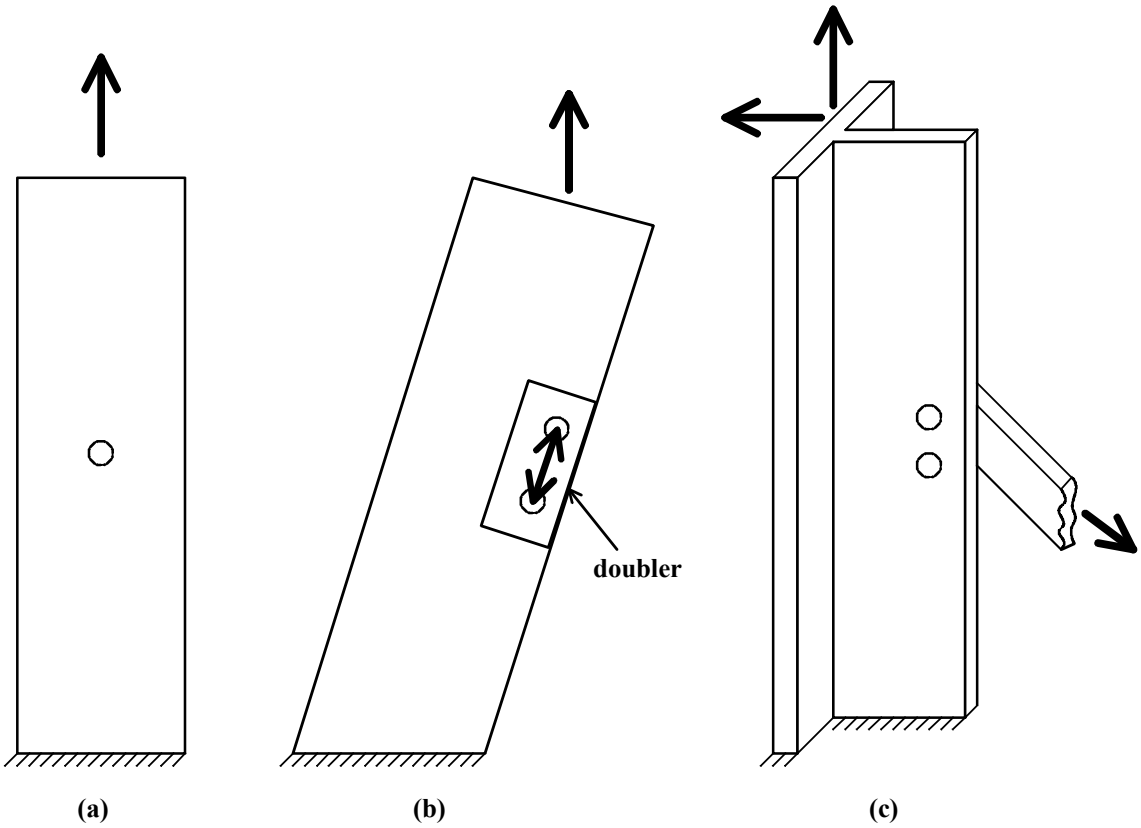

Figure 2. Schematics of mechanical test specimens containing holes.

Materials Characterization

Ideally, specimens would be machined from the same lot of material used for the tank construction, but no such material was available. Instead, specimens were machined from aluminum alloy 2014 plate material nominally 1.5 inches (38 mm) thick. The nominal chemical composition of 2014 aluminum, both the tank material and the plate used in this study, is listed in Table 1.

The material obtained for this study is similar to that of the tanks, although subtle differences in processing may exist. Samples were removed from the plate and examined using optical microscopy. This was also done to examine material from a qualification tank and two additional tanks, denoted here as tank #6 and tank #10. Optical metallographs of samples were cut from several locations through the material thickness. Images corresponding to (a) the material used for this study, (b) the qualification tank, (c) tank #6, and (d) tank #10 near the plate surfaces (t/16)1are shown together for comparison in Figure 3. The images shown correspond to the same plate orientation and magnification. With regards to the

[1] Plate depth is described here relative to the plate thickness, t. For example, t/16 would correspond to material that is 1/16 of the plate thickness from the free surface.

average microstructural dimension, it appears that the grain size for the material of tank #6 (Figure 3c) is significantly larger than the others. In comparison, little difference is observed between microstructural scales of tank #10 (Figure 3d), the material used for this study (Figure 3a), and the qualification tank (Figure 3b). The images in Figure 3 are normal to the longitudinal (L) plate direction, such that the plate short-transverse (S) direction is vertical and the long-transverse (T) direction is horizontal.

Optical metallographs of samples taken near the plate centerline (t/2) are shown in Figure 4. Images corresponding to (a) the material used for this study, (b) the qualification tank, (c) tank #6, and (d) tank #10 are shown together for comparison. The variation in microstructure seen here is similar to that of Figure 3. Specifically, the grains depicted for the tank #6 material appear to be coarse (Figure 4c) and little difference in microstructural scale is observed between tank #10 (Figure 4d), the material used in this study (Figure 4a), and the qualification tank (Figure 4b). The images in Figure 4 are normal to the longitudinal (L) plate direction, such that the plate short-transverse (S) direction is vertical and the long-transverse (T) direction is horizontal.

Mechanical Properties

Mechanical properties tests were conducted to establish the appropriate input for analytical studies (i.e., elastic modulus, yield stress, fracture toughness, etc.) for the plate product used in this study. Samples were tested in multiple orientations to determine the nature of the material anisotropy and to determine the appropriate parameters for a given product orientation. Mechanical testing was comprised of tensile tests and fracture toughness tests, because these results were considered to be of interest to the tank cracking problem.

Table 1. Nominal chemical composition of aluminum alloy 2014 plate used for study.

	Nominal	**min**	**max**
Silicon (Si)	0.75%	0.50%	1.20%
Iron (Fe)	0.23%	-	0.70%
Copper (Cu)	4.10%	3.90%	5.00%
Manganese (Mn)	0.72%	0.40%	1.20%
Magnesium (Mg)	0.45%	0.20%	0.80%
Chromium (Cr)	0.01%	-	0.10%
Zinc (Zn)	0.14%	-	0.25%
Titanium (Ti)	0.04%	-	0.15%
Aluminum (Al)	balance		

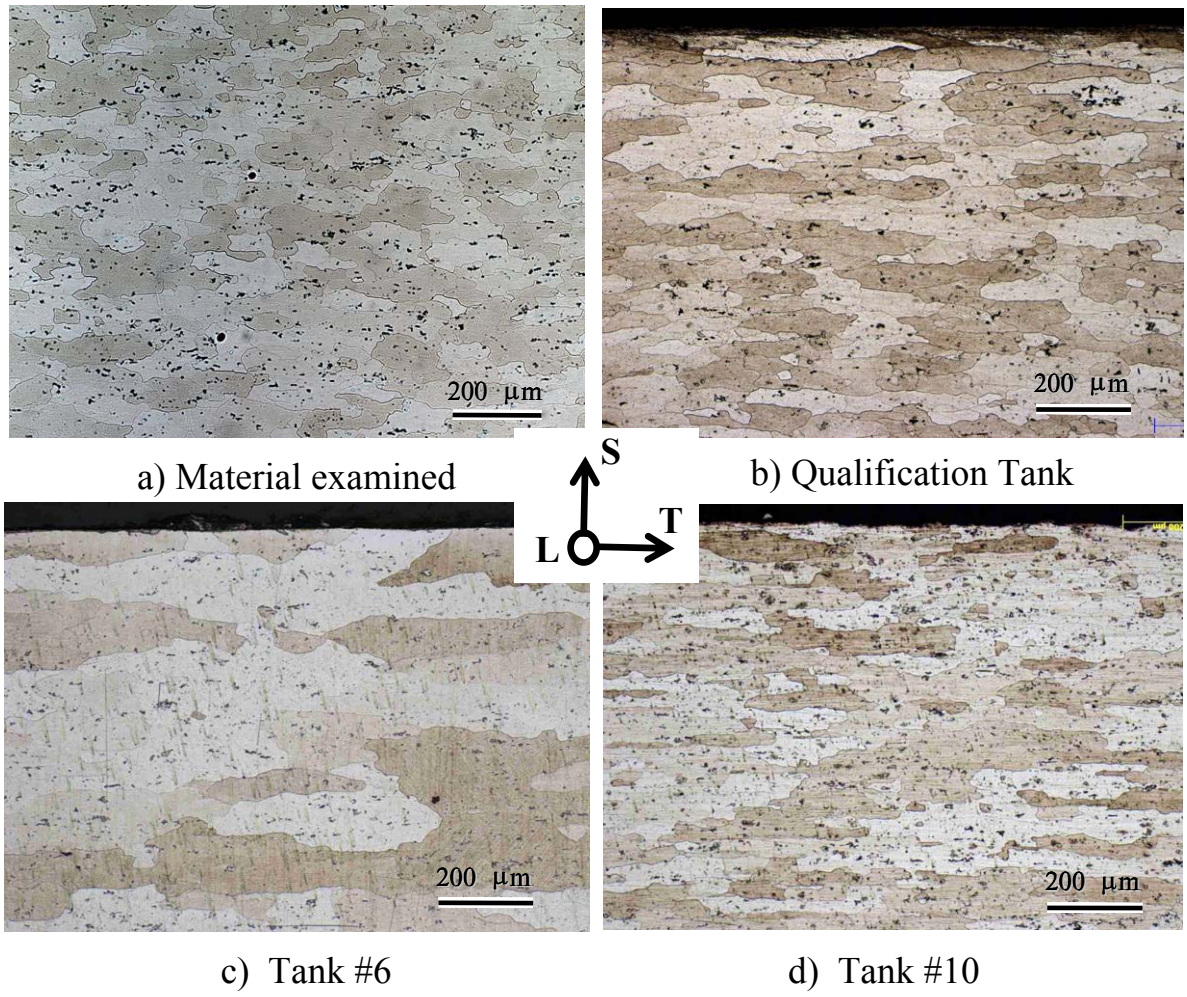

Figure 3. Optical metallographs of 2014 aluminum samples taken near the plate surface (t/16) for (a) the product acquired for this testing program, (b) the qualification tank, (c) tank #6, and (d) tank #10.

Tensile Testing

Tensile testing was conducted using the dog-bone specimen configurations shown in Figure 5. To better simulate the geometry of the isogrid rib, these specimens deviated slightly from the standard configuration supplied in American Society for Testing and Materials (ASTM) standard E-8 (ref. 1). Specifically, the width and thickness of the specimen gage section was made nearly identical to the dimensions of the integral stiffener, 0.885 inches (22.5 mm) and 0.105 inches (2.67 mm), respectively. However, all testing conditions, i.e. initial strain rate, were in compliance with ASTM standard E-8. The gage section of the first tensile specimen (See Figure 5a) was centered on the plate centerline and will be referred to as t/2 tensile specimens (where t is the plate thickness). After testing these specimens, it was revealed that the region of concern (stiffener hole location) was located closer to the free edge of the plate, near the t/4 plate position. A second tensile specimen configuration (See Figure 5b) was designed such that one edge of the gage section coincides with the surface of the plate, and will be referred to as the t/4 tensile specimen configuration. To better understand the stress/strain concentration effect on the 2014 plate material behavior due to the fastener holes, half of the L-oriented tensile specimens tested contained a countersink hole in the center of the gage section. A detail of the hole configuration is shown in Figure

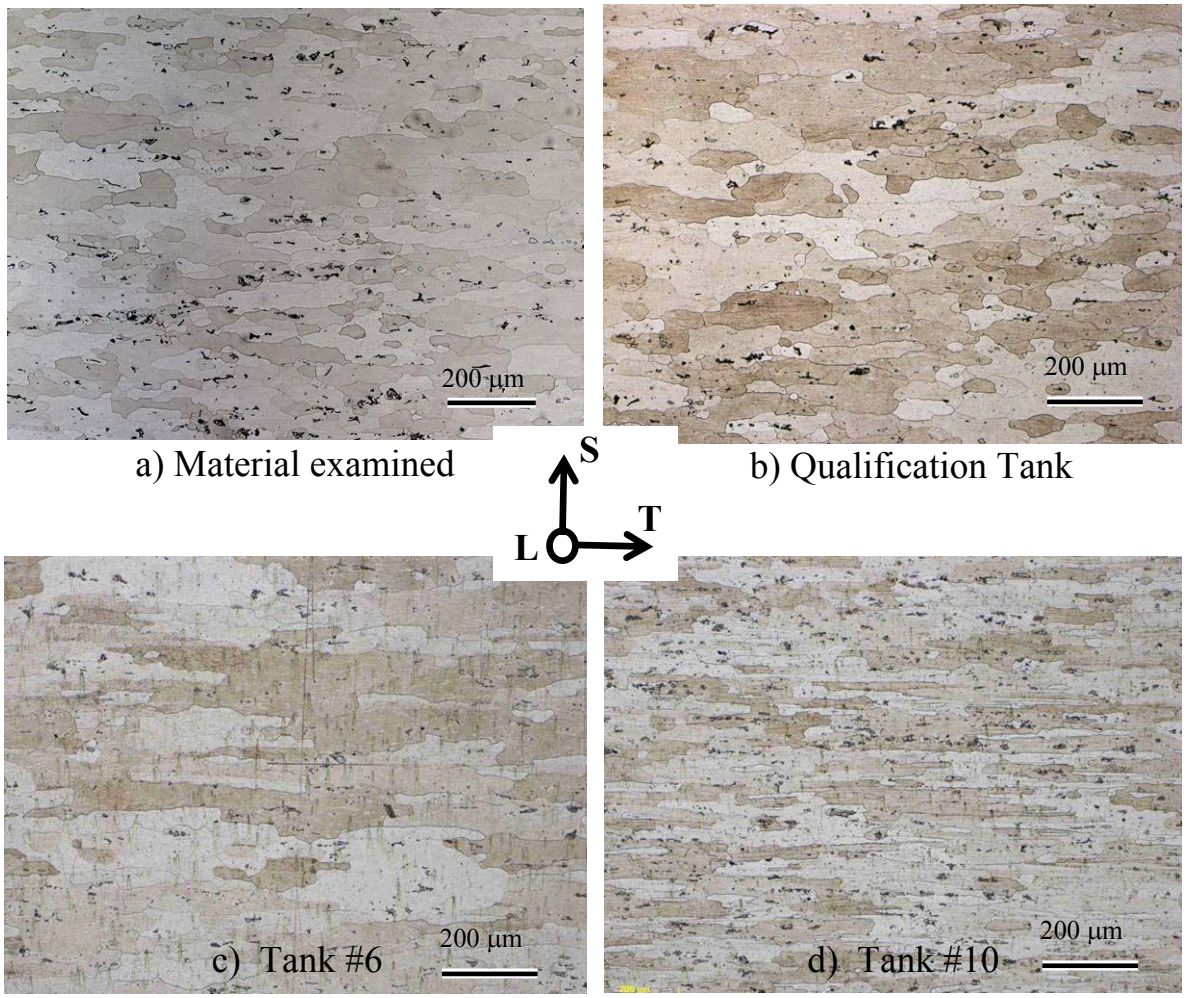

Figure 4. Optical metallographs of 2014 aluminum samples taken near the plate center-line (t/2) for (a) the product acquired for this testing program, (b) the qualification tank, (c) tank #6, and (d) tank #10.

5c. Plots of stress versus strain for the L-oriented tensile specimens are supplied in Figure 6 and the test results are summarized in Table 2. A comparison of the t/2 and t/4 tensile results reveals no significant differences in mechanical behavior. Specimens with a countersink hole in the specimen gage section reveal a significant reduction in ductility due to the stress/strain concentration near the fastener hole.[2] Here, stress was calculated using the net section area, and this information was used in the analyses described in this document. For all specimens, gage section strain was measured using a 2-inch extensometer centered in the gage section (for specimens without holes) or centered about the hole.

Additional tensile testing was performed using specimens machined in the plate-thickness direction to determine the tensile properties normal to the plane of the plate. Variation in tensile properties with plate orientation could significantly affect the damage progression in the material. As the plate used was nominally 1.5 inches (38 mm) thick, small specimens were used, as shown schematically in Figure 7. A total of six S-oriented tensile specimens were tested. Stress-versus-strain data are shown in Figure 8, and the data is summarized in Table 3.

[2] Strain at specimen failure is considered a good indication of ductility. Specimens without holes failed at global strain levels nearly 10 times greater than for specimens with holes.

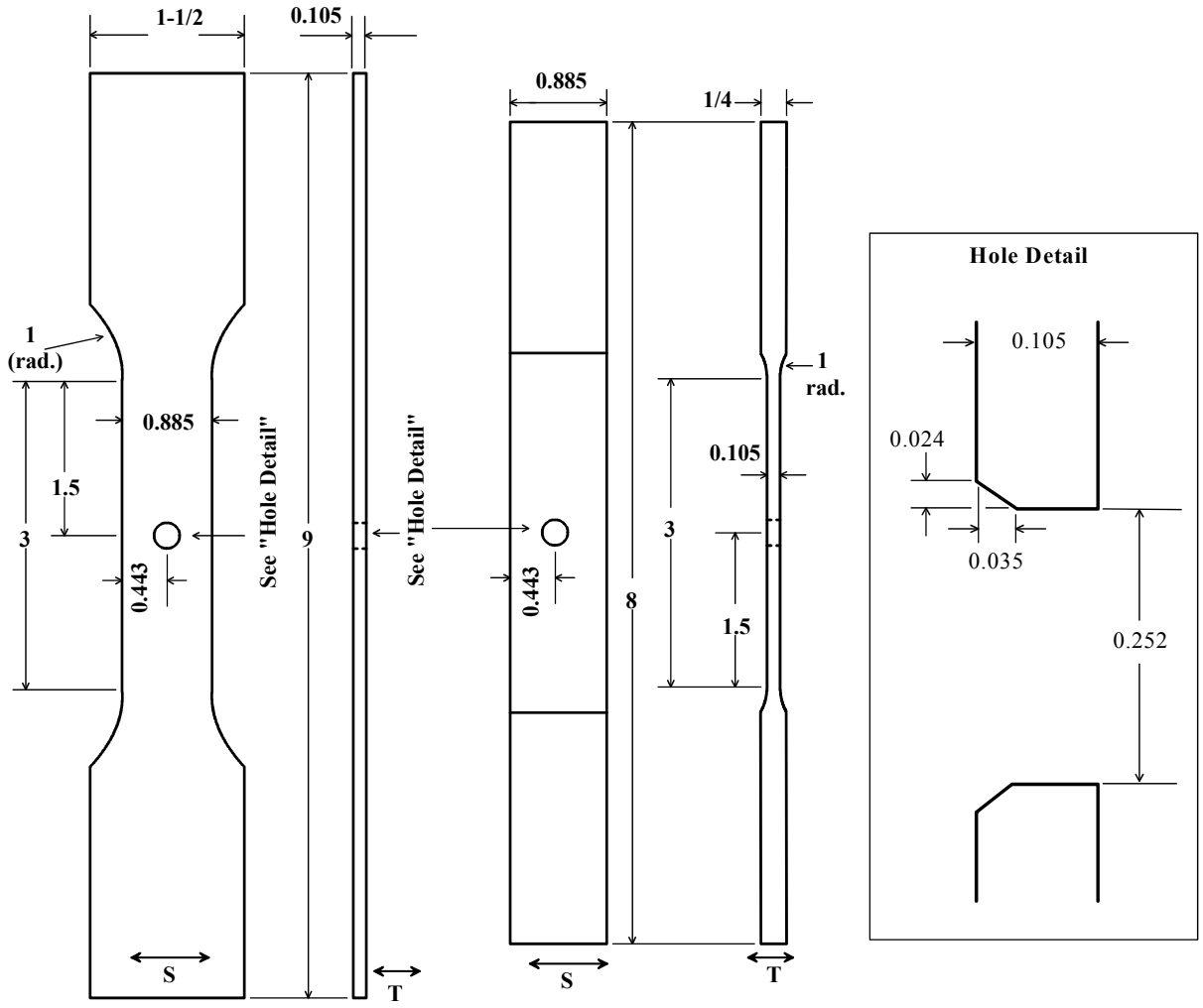

(a) t/2 specimen (b) t/4 specimen (c) hole detail

Figure 5. Tensile specimen configurations. All dimensions inches.

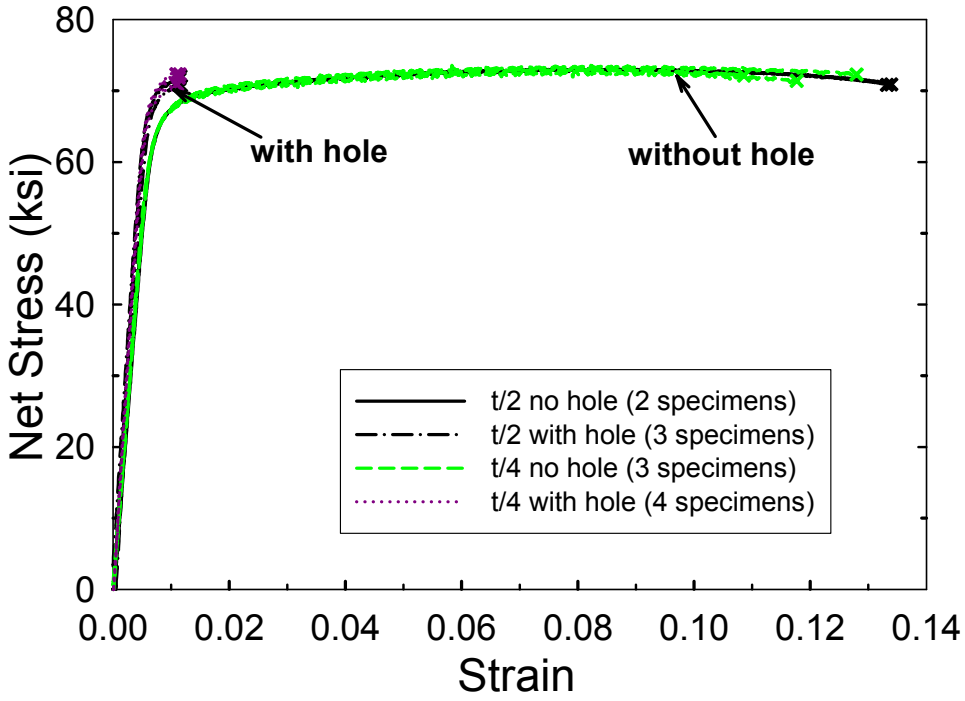

Figure 6. Tensile test data for L-oriented tensile specimens.

Table 2. Tensile test results for L-oriented specimens.

	Ultimate Stress ksi (MPa)	**Strain %**
t/2 (no hole)	73.52 (506.9)	13.39
	73.51 (506.8)	13.37
t/2 (with hole)	72.79 (501.9)	1.135
	72.51 (500.0)	1.155
	71.37 (492.1)	1.145
t/4 (no hole)	73.30 (505.4)	11.78
	73.60 (507.5)	10.80
	74.11 (511.0)	12.79
t/4 (with hole)	73.01 (503.4)	1.160
	73.12 (504.2)	1.095
	72.59 (500.5)	1.130
	71.53 (493.2)	1.100

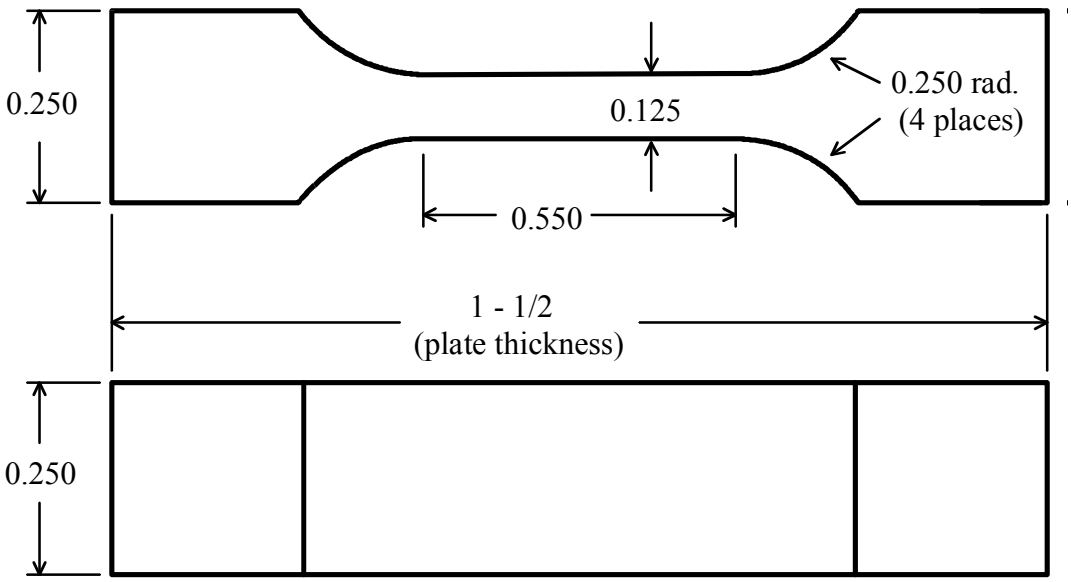

Figure 7. Short transverse (S) oriented tensile specimen configuration. All dimensions inches.

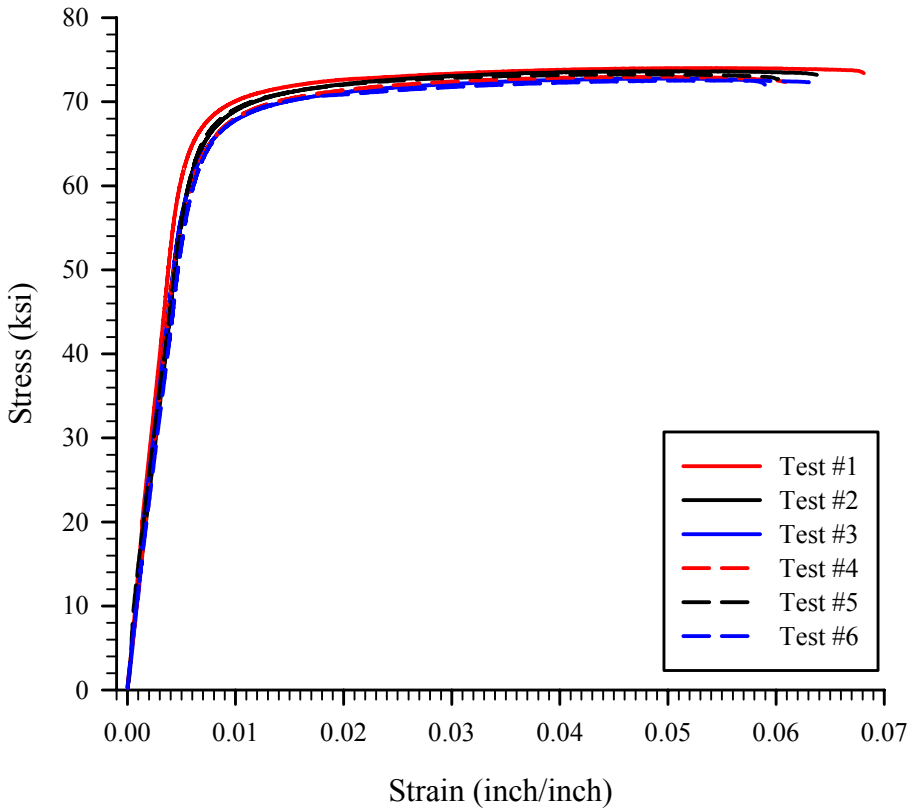

Figure 8. Tensile test data for S-oriented tensile specimens.

Table 3. Summary of tensile test properties for S-oriented specimens.

	Ultimate Stress ksi (MPa)	Strain %
	73.64 (507.8)	6.4
	74.02 (510.4)	6.8
	72.77 (501.8)	5.9
	72.98 (503.2)	6.1
	73.27 (505.2)	6.0
	72.21 (497.9)	6.4
Average	**73.21 (504.8)**	**6.3**

Fracture Toughness Testing

Fracture toughness testing was performed using compact tension (C(T)) specimens machined from the 2014 plate material. Specimens were machined in two orientations (S-T and T-S), as shown schematically in Figure 9.

It was desired to produce plane-strain fracture toughness values, K_{Ic}, in accordance with ASTM standard E399 (ref. 2), however, there was concern that the specimen geometry may not allow this. To satisfy ASTM E399, the specimen thickness, B, and the crack length, *a*, must satisfy the following criteria,

$$B, a > 2.5\left(\frac{K_{Ic}}{\sigma_y}\right)^2$$

where σ_y is the 0.2% offset yield stress, which is approximately 64 ksi (440 MPa) for 2014 aluminum plate material. Considering that B = 0.5 inches, the values of fracture toughness will satisfy the plane-strain criteria for K < 28.6 ksi√in. As this value is near typical K_{Ic} values for aluminum alloys, it was not certain that the fracture toughness values obtained from these tests would satisfy the geometry constraints of ASTM standard E399. Therefore, tests were performed in accordance with the more general non-linear elastic-plastic test method of ASTM E1820 (ref. 3) to ensure that valid test results would be obtained.

Specimens were precracked by fatigue loading at K_{max} = 10 ksi√in (11 MPa√m) and R = 0.1 until a crack length of approximately *a* = 0.6 inches was achieved (*a*/W = 0.5). This required between 35,000 and 40,000 cycles for S-T specimens and between 60,000 and 70,000 cycles for T-S specimens. After specimens were precracked, fracture toughness tests were performed by loading specimens at a constant stroke rate of 0.01 inch/minute. Crack length was determined during the tests by monitoring a crack mouth displacement gage during periodic unloading. Typical load versus displacement data are plotted in Figure 10 for both S-T and T-S specimens. A nearly linear relation between applied load and crack-mouth displacement is initially seen during the tests. The peak load that the specimen carries occurs nearly immediately after the load-displacement relation becomes non-linear, such that the peak load corresponds to P_Q (candidate toughness load, to be determined if plane-strain requirements are satisfied).

Thus, the corresponding K_Q values are the K_{Ic} values for this material since the plane-strain criteria are also satisfied. K_{Ic} data for all tests are listed in Table 4. Three fracture tests were performed for each orientation. Initial specimen geometry (thickness, B, and width, W) and the initial crack length, a_i, are also listed.

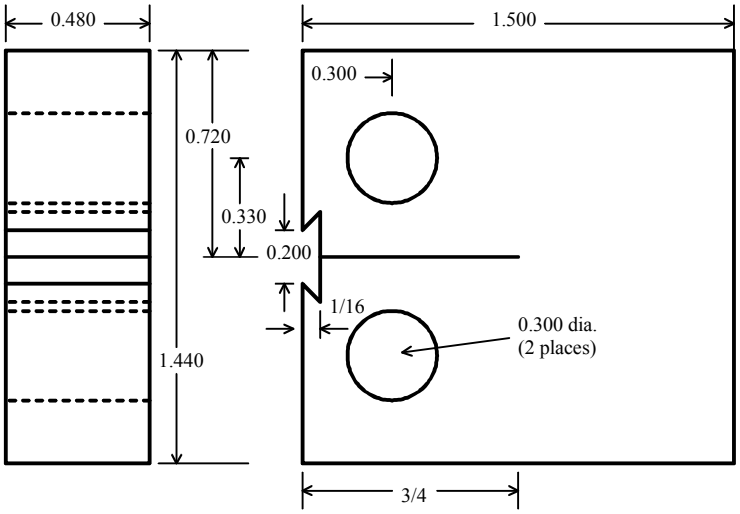

(a) C(T) specimen

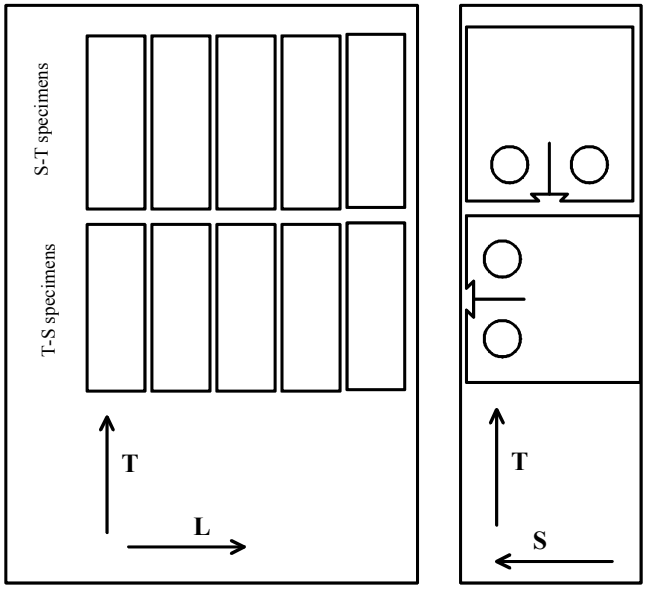

(b) Specimen orientations

Figure 9. Schematics of C(T) specimens used for fracture toughness testing. (a) C(T) specimen configuration. (b) Schematic showing the two orientations of specimens used in this study. All dimensions inches.

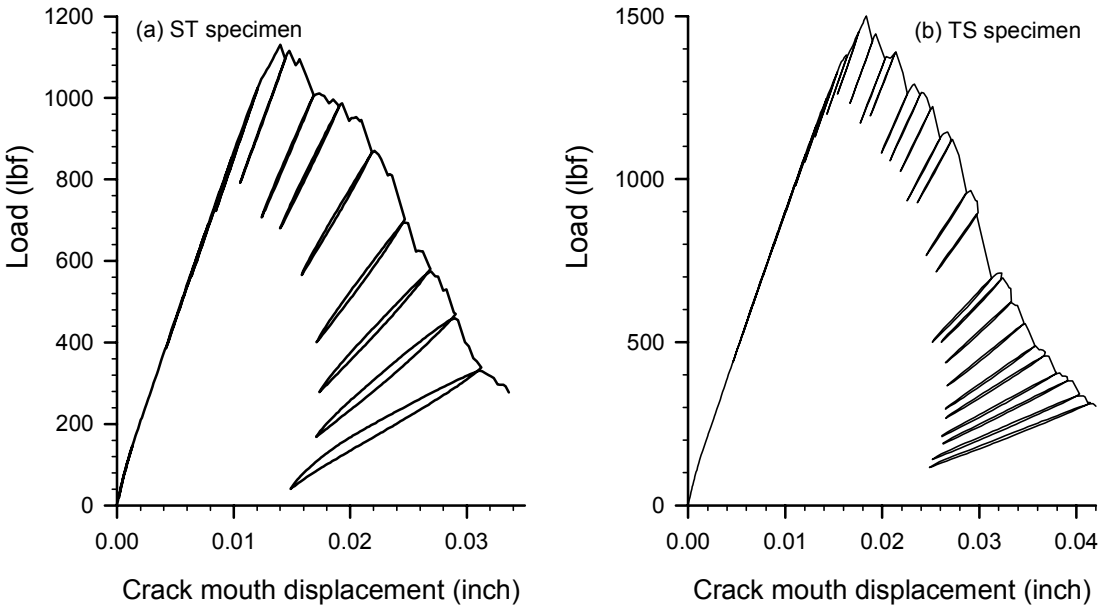

Figure 10. Typical load-versus-crack-mouth-displacement test data for an (a) S-T specimen and (b) T-S specimen.

Table 4. Fracture toughness test results.

Specimen	B (inch)	W (inch)	a_i (inch)	P_Q (lb_f)	K_{Ic} (ksi√in)
ST-1	0.480	1.119	0.596	1,130	23.8
ST-2	0.478	1.200	0.598	1,116	20.5
ST-3	0.479	1.200	0.601	1,156	21.3
TS-1	0.474	1.200	0.595	1,481	27.2
TS-2	0.475	1.202	0.596	1,501	27.5
TS-3	0.476	1.201	0.594	1,502	27.4

Simulation of Service Cracking

Initial attempts to simulate service cracking by performing uniaxial tension specimens with a hole in the center of the specimen, as indicated in Figure 5a, resulted in catastrophic failure at the holes normal to the loading axis. Due to the symmetry of these specimens, the stress state on each side of the holes was identical and failure occurred nearly simultaneously on both sides of the specimen. (See Figure 11) However, this is not what was observed during tank testing where asymmetric cracking and significant post-cracking load carrying capability occur.

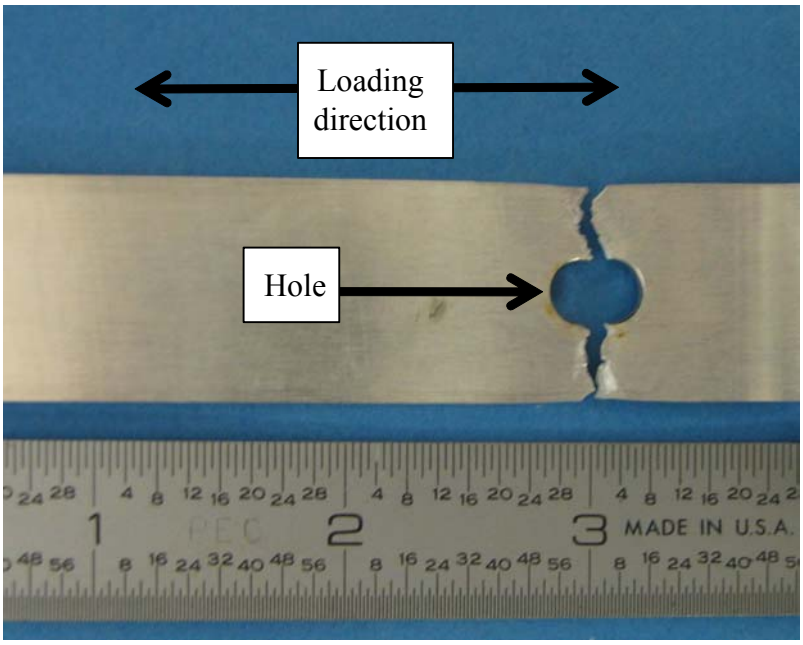

Figure 11. Photograph of failed uniaxial tension specimen with center hole.

Reproducing service cracking with a uniaxial specimen with a centered hole was believed to have failed because of specimen symmetry. Further, this specimen was believed to be an overly simplified representation of the tank structure because it contained a single hole and did not permit hole-to-hole cracking or loading through the holes. Therefore, a non-symmetric two-hole specimen was designed, as shown in Figure 12. The specimen was loaded in a servo-hydraulic test machine with the specimen axis oriented 18^{o} from the loading axis as shown in Figure 13. One end of the specimen was cut at an 18^{o} angle to help ensure consistent specimen alignment. Specimens were angled in an attempt to reproduce observed cracking in tank structures which occurred at an angle of approximately 18^{o} with respect to the isogrid rib. Aluminum stiffeners were attached on each side of the specimen, connected through two pins. The stiffeners could be adjusted by tightening the end caps to ensure a small pre-load before loading the specimen. As the specimen is loaded the spacing between the two holes is expected to increase, however, the stiffeners will constrain this displacement and carry additional load.

Cyclic loading under high plastic strain was performed to determine if severe cyclic loading, similar to what occurs during pressurization testing, could initiate cracks. The motivation for this testing was to challenge the presumption that no significant cracking occurs prior to the formation of a primary crack. A plot of load versus extension is shown in Figure 14. Here, one specimen was loaded under monotonic loading to failure. A second specimen was loaded cyclically with limited strain (severe plastic deformation, but well below the strain at which failure would be expected based on the results of the first specimen tested) applied during each cycle. A total of 29 cycles was applied to the specimen. The specimen was removed from the load frame periodically (a total of 13 times) and the interior of the hole surfaces was examined in a scanning electron microscope (SEM) to inspect for damage progression (See X symbols in Figure 14). Here, damage consistent with that indicated in Figure 15 is observed by the first inspection of the hole surfaces. While some limited damage progression has been observed with increased loading cycles, a clear determination of damage evolution could not be developed through the serial SEM observations.

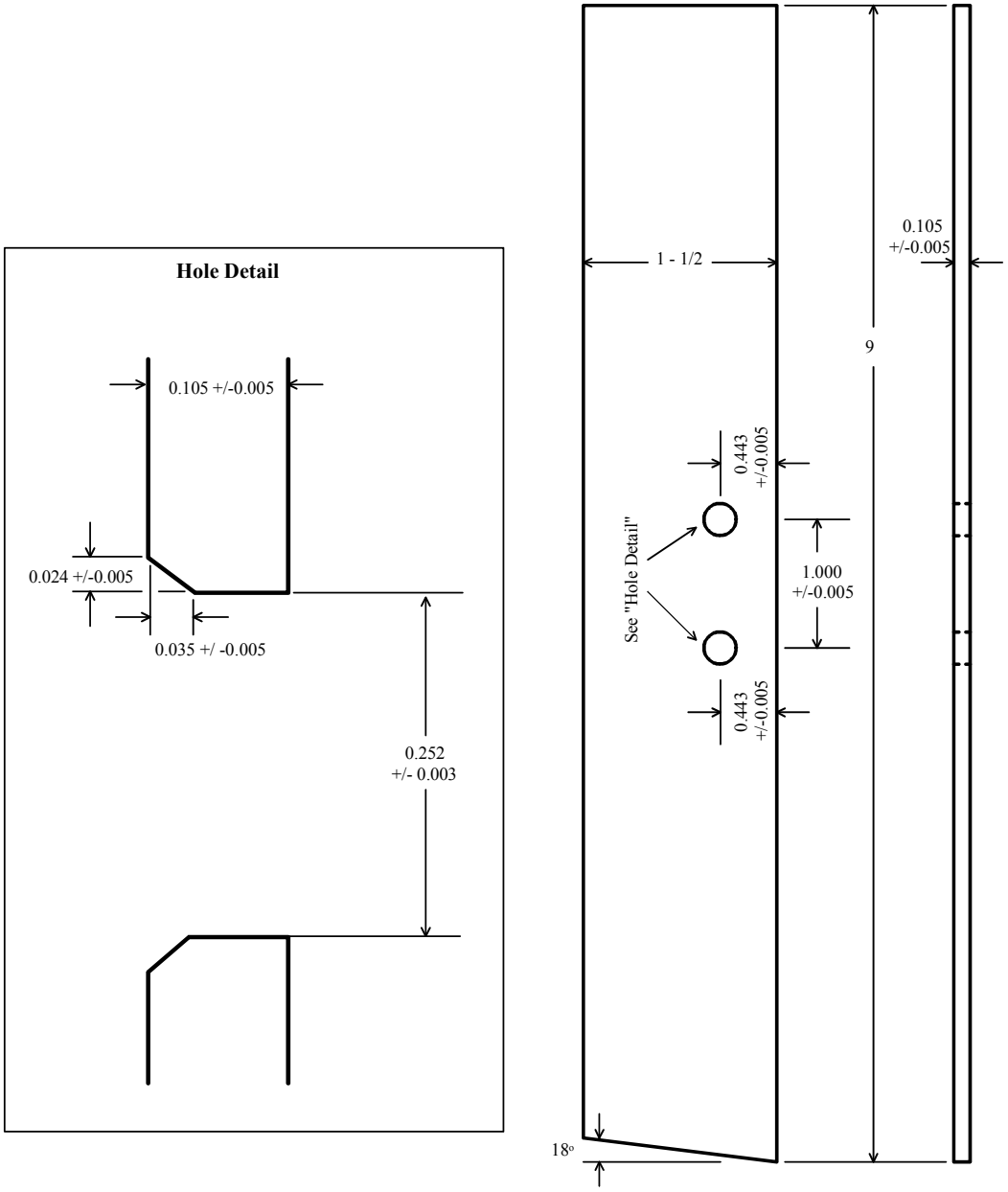

Figure 12. Schematic of two-hole specimen. All dimensions inches.

For all tests on 2-hole specimens, failure occurred as a fracture across the entire specimen width breaking the specimen into two pieces. It was hoped that testing under displacement control would allow a progressive failure such that a primary crack would occur first (cracking from one hole to the surface nearest the hole), possibly with an angled secondary crack on the opposite side of the hole, as observed in service. Unlike the integrally-stiffened tank, the 2-hole specimen did not have any geometric discontinuity to arrest a crack once it started to propagate. Additionally, strain gages placed on the aluminum doublers indicated limited by-pass loading (less than 5%) from pin to pin, suggesting that this configuration was not adequate to represent the complex loading condition about a fastener hole in an isogrid rib. This problem was resolved with another specimen better designed to reproduce loading conditions based on a detailed analysis of the local stress state.

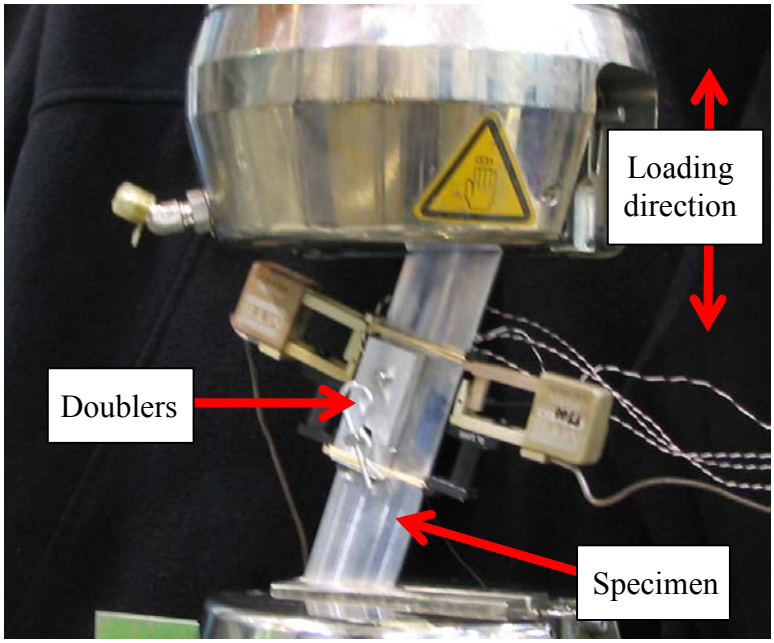

Figure 13. Photograph of two-hole specimen in servo-hydraulic test machine.

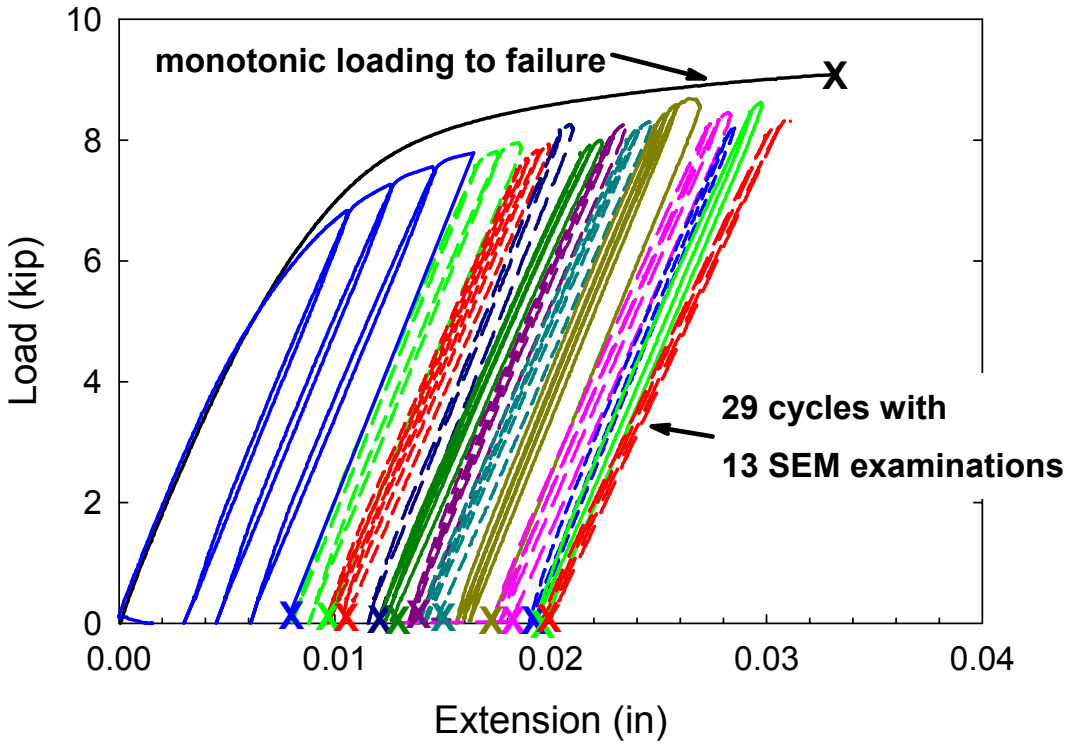

Figure 14. Plot of load-strain data for cyclic loading of 2-hole specimen

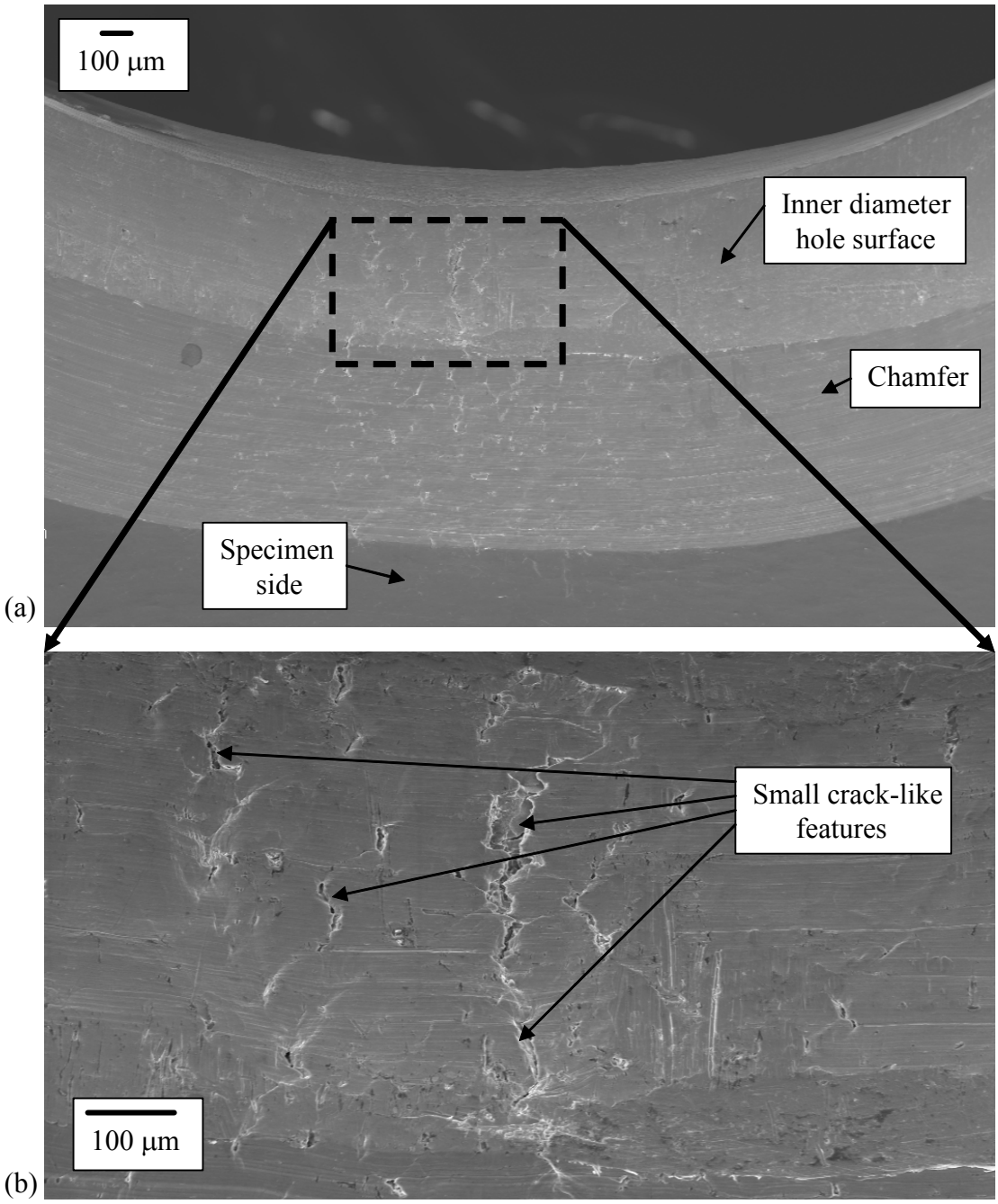

Figure 15. SEM micrographs of holes during fatigue loading; (a) Photograph of hole ID; (b) High-magnification image of crack-like damage on hole ID.

Testing of 3-D Specimen

Based on analytical results (see Appendix), a modified 2-hole specimen was designed to better simulate the three-dimensional (3-D) geometry and stress state, as shown schematically in Figure 16. To achieve the desired ratio of axial load and pin-bearing load, the specimen was tested using the axial tension and bending (ATB) test machine at Langley Research Center (ref. 4). A photograph of a

specimen mounted in the ATB machine is shown in Figure 17. Here, one end of the test specimen is fixed and the other end is attached to a clevis connected to two servo hydraulic actuators to apply axial and transverse forces. The pin loading that is expected for the fastener hole of an isogrid rib attached to a stiffener is simulated by affixing the top fastener hole of the specimen to a fixed block using a steel stiffener measuring 0.185" in thickness. The stiffener has two strain gages applied to the mid-section to estimate pin loading during a test. Specimen loading is accommodated by applying constant displacement for both the axial and transverse actuators.

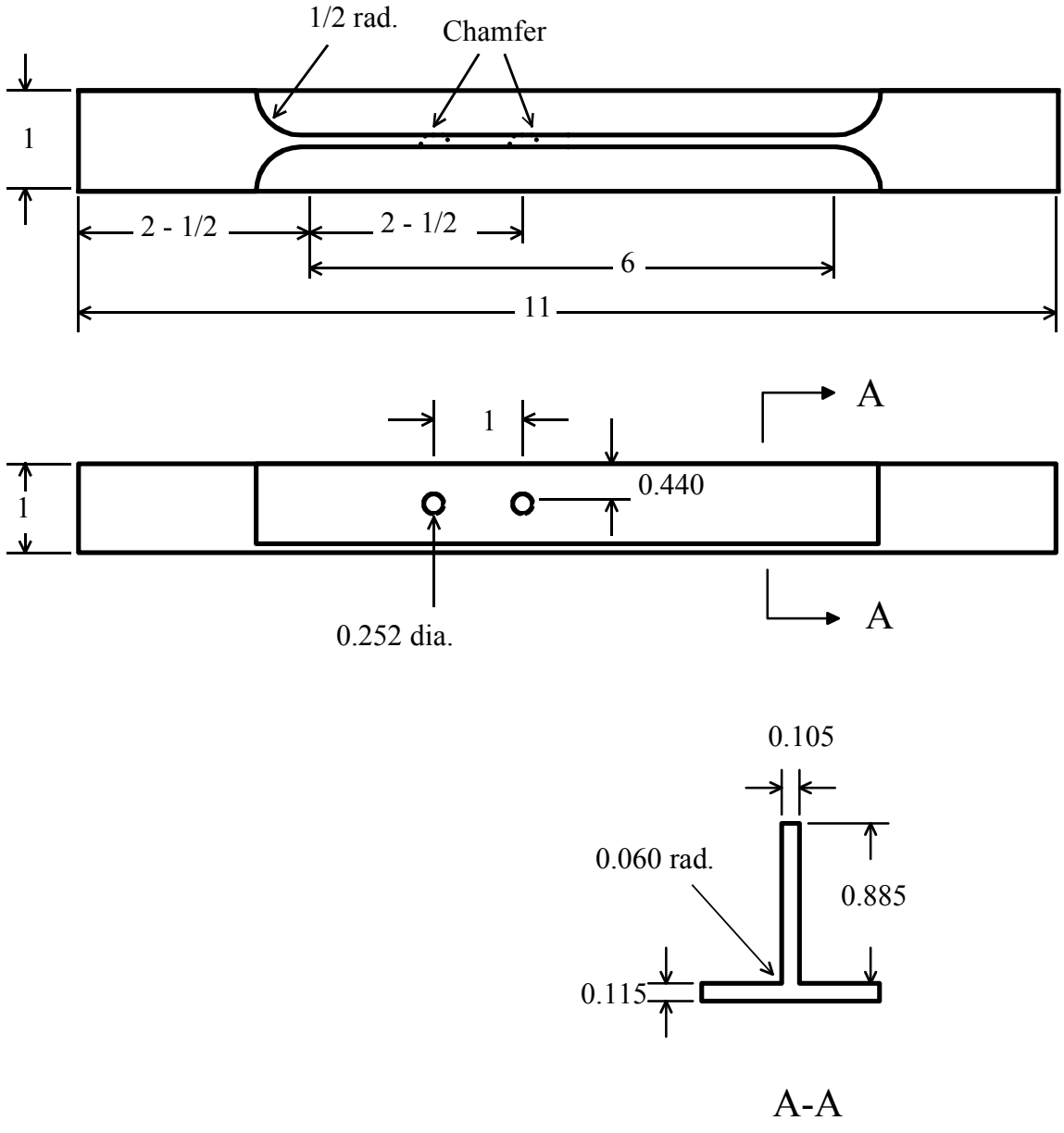

Figure 16. Schematic of 3-D specimen. All dimensions inches.

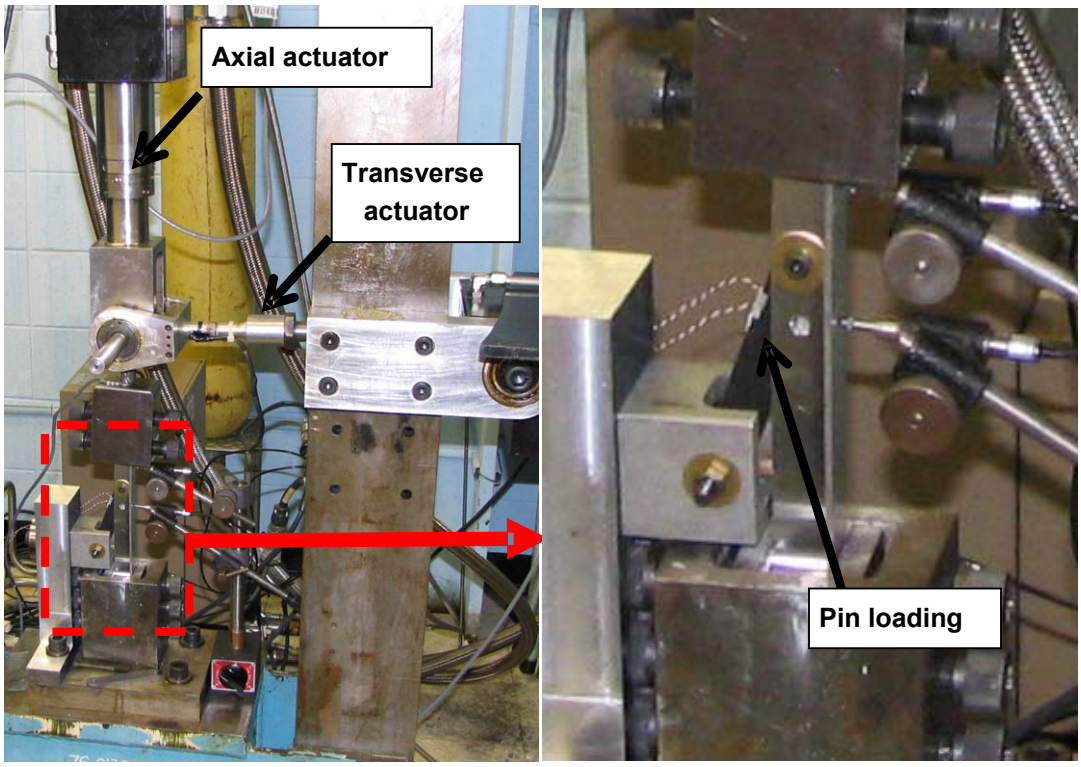

(a) ATB test setup (b) Specimen in ATB

Figure 17. Photo of 3-D specimen mounted in test machine.

Mechanical testing of the 3D specimens in the ATB facility was performed at three different displacement ratios (5:1, 10:1, and 20:1, axial to transverse displacement ratio). Loading of the first 3-D test specimen at a 5:1 displacement ratio was terminated well before fracture due to insufficient pin loading. As the specimen was loaded, the axial-to-pin load ratio rapidly approached 10:1 (due to the specimen having a transverse compliance significantly greater than the integrally-stiffened tank structure). This result indicated that a higher displacement ratio was required. Data for a 10:1 displacement ratio is supplied in Figure 18. Here, the loads measured from the load cells for the axial and transverse actuators and the load determined for the pin loading increase with increasing displacement until a fracture event occurs at a transverse displacement slightly greater than 0.42 inch. The maximum axial load was 6.89 kip (30.6 kN), while the maximum transverse and pin loads were 0.36 kip (1.60 kN) and 0.79 kip (3.51 kN), respectively. The primary crack ruptured through to the free surface, while the secondary crack propagated to the web formed by the simulated skin (See Figure 19). On one of the surfaces, the secondary crack propagated at an angle from the loading axes, similar to that observed in service (See Figure 19a), however, on the other side of the specimen, the secondary crack initially propagates normal to the axial direction (See indicated region in Figure 19b), which is inconsistent with the crack morphologies observed in service. This specimen was loaded to failure to observe the complete fracture morphology. An optical metallograph of both fracture surfaces is shown in Figure 20. The secondary crack propagated through the entire rib section and has nearly penetrated the 0.115-inch skin material.

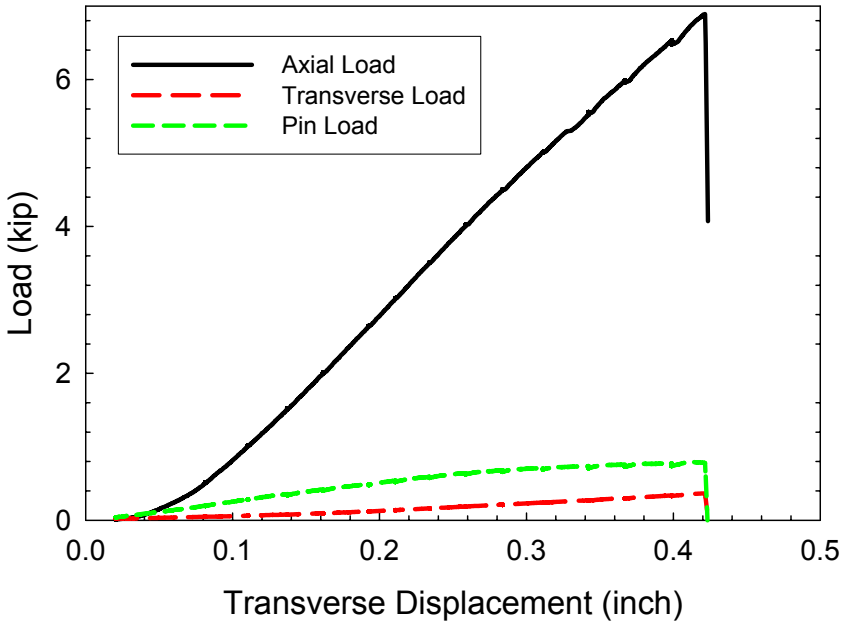

Figure 18. Load-versus-displacement data for specimen tested at a transverse to axial displacement ratio of 10:1.

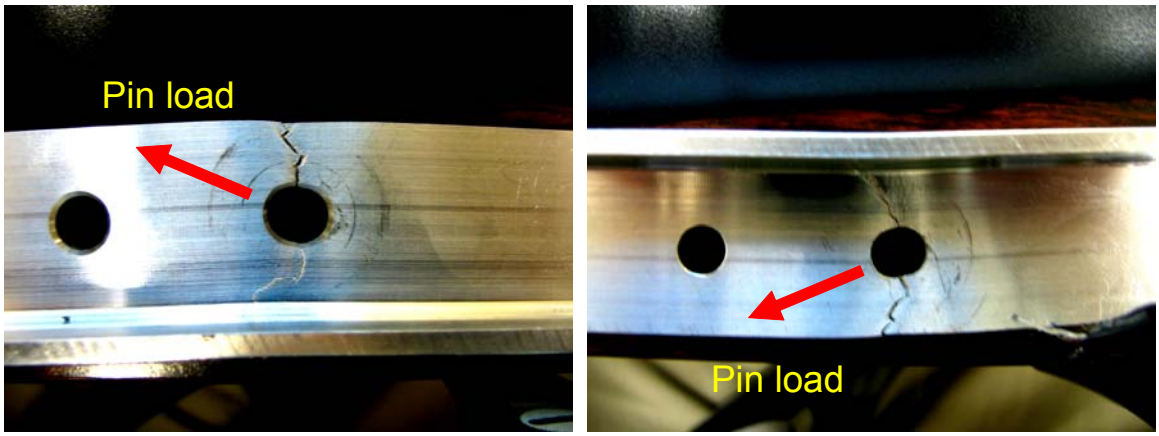

(a) Photograph of specimen front.

(b) Photograph of specimen back.

Figure 19. Specimen surfaces of fractured 3-D specimen tested at a transverse to axial displacement ratio of 10:1. For the photographs shown, the axial loading direction is horizontal.

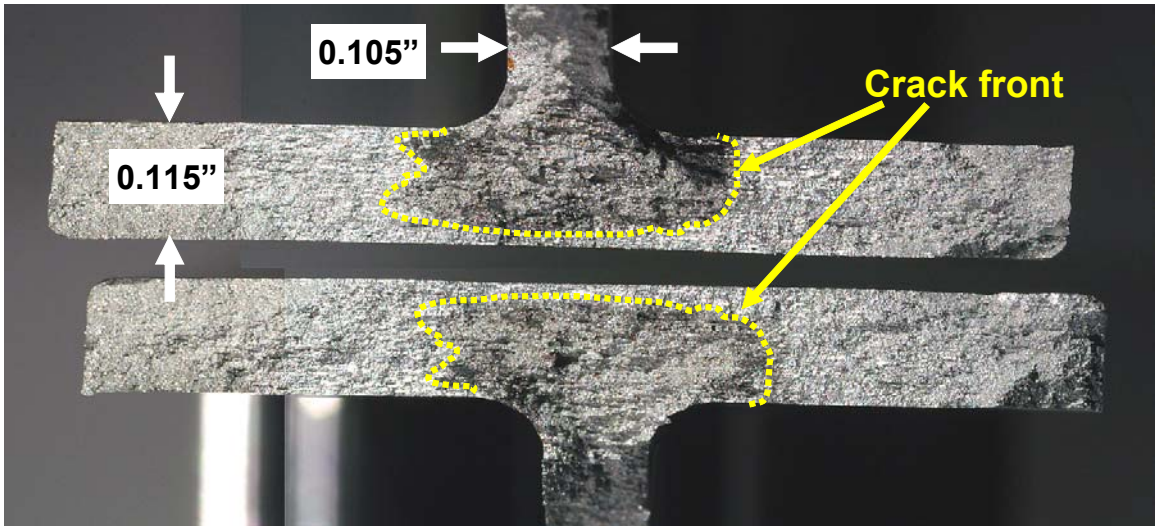

Figure 20. Optical metallograph of secondary-crack fracture surfaces of 3-D specimen tested at a transverse to axial displacement ratio of 10:1.

Due to the relatively high axial-to-pin displacement ratio (8.7:1) required to reproduce the crack configuration in the failed tanks, and the crack morphology realized at a displacement ratio of 10:1, additional tests at a displacement ratio of 20:1 were performed. Data for one of the 20:1 tests are supplied in Figure 21. Here, the loads measured from the load cells for the axial and transverse actuators and the load determined for the pin loading increase with increasing displacement until a fracture event occurs at a transverse displacement slightly greater then 0.60 inch. The maximum axial load was 4.94 kip (22.0 kN), while the maximum transverse and pin loads were 0.39 kip (1.73 kN) and 0.96 kip (4.27 kN), respectively. Therefore, the pin loading was more than 20% greater for the 20:1 tests than was observed for the 10:1 test in Figure 18. Images of the specimen surfaces are shown in Figure 22. Here, the secondary crack was observed to grow at an angle to both the axial and transverse load lines, and the crack did not penetrate the simulated skin surface. For two specimens tested under this condition, the secondary cracks were greater than 0.050 inch (1.3 mm) from the skin material. This means that for the 20:1 axial-to-pin displacement loading, the secondary cracking was less severe than for 10:1 axial-to-pin displacement testing. A summary of data for the 10:1 and 20:1 tests are listed in Table 5.

Table 5. 3-D specimen test data for ATB testing.

Displacement Ratio *	Max Axial Load, kips (kN)	Max Transverse Load, kips (kN)	Max Pin Load kips (kN)	Max Transverse displacement in (mm)
10:1	6.89 (30.6)	0.36 (1.60)	0.79 (3.51)	0.42 (10.7)
20:1	4.94 (22.0)	0.39 (1.73)	0.96 (4.27)	0.61 (15.5)
20:1	5.33 (23.7)	0.39 (1.73)	0.97 (4.31)	0.58 (14.7)

* Transverse:Axial displacement ratio

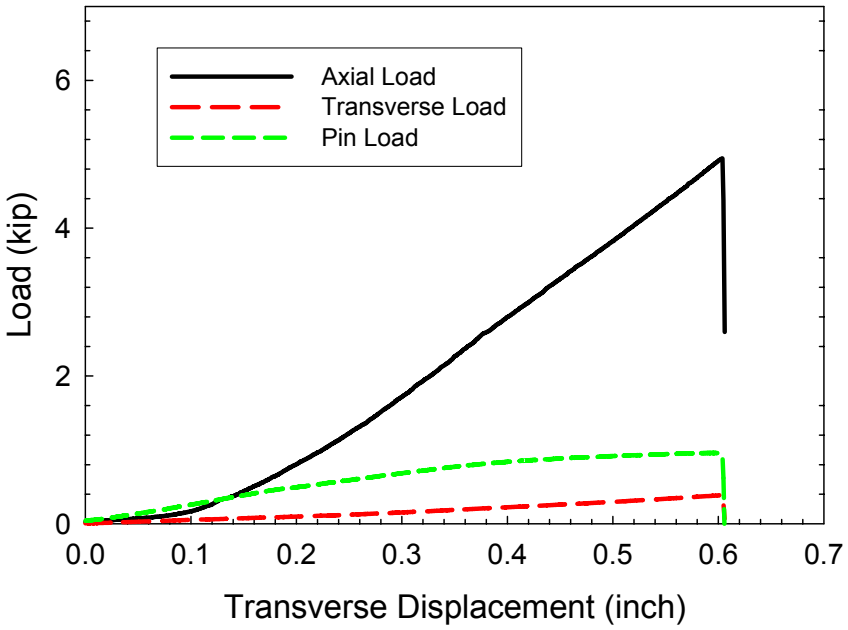

Figure 21. Load-versus-displacement data for specimen tested at a transverse to axial displacement ratio of 20:1.

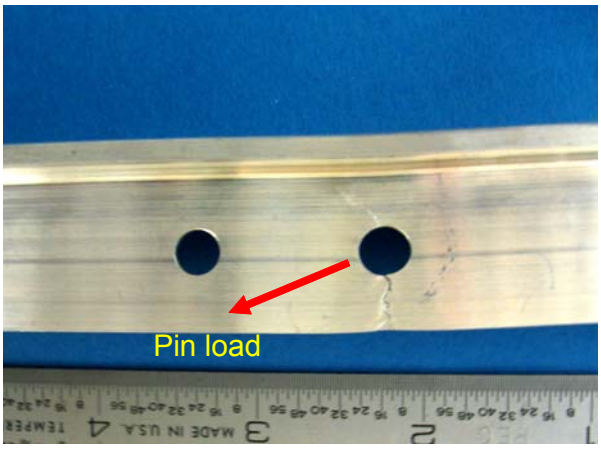

(a) Photograph of specimen front.

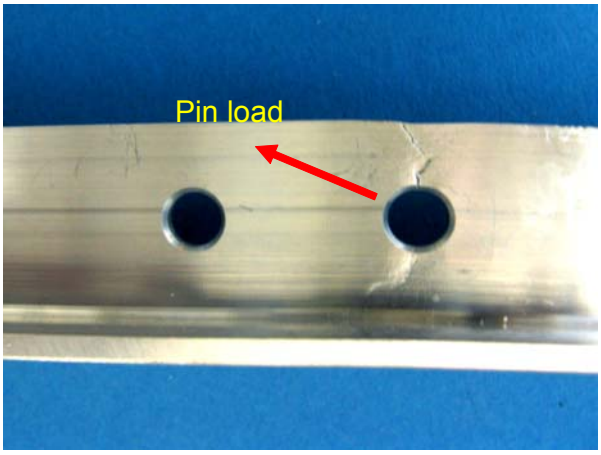

(b) Photograph of specimen back.

Figure 22. Specimen surfaces of fractured 3-D specimen tested at a transverse to axial displacement ratio of 20:1. For the photographs shown, the axial loading direction is horizontal.

Summary

The objective of this study was to simulate the fracture morphology observed in service to develop a better understanding of the damage sequence that can be expected during pressurization of the tanks under investigation. A more complete understanding of the damage processes can then be used to assist in developing rational for continued use.

Testing was performed on commercially available product forms of aluminum alloy 2014, the alloy used for tank construction. Metallographic examinations along with material property testing were performed to ensure that the material used in this study was typical of that used to manufacture the tanks.

Mechanical tests were performed with multiple specimen designs to better simulate the local geometry and stresses. Cyclic testing of the 2-hole specimen under high local strains indicated that visually detectable cracks are not likely prior to failure. This observation supports but does not prove the assumption that the formation of primary cracks is the result of a single event, not the product of accumulated damage.

Damage in specimens closely resembling the tank pressurization cracking was obtained through the use of specimens that capture the local three-dimensional geometry under representative loading. Specifically, both specimen and service cracking events produced a primary crack that severed the ligament from a fastener hole to the interior surface of the rib. Secondary cracks, which are angled with respect to the tank wall, were also observed and appeared to arrest as the crack approached the skin of the tank. Although laboratory specimens lack the surrounding structure to simulate the post-cracking load redistribution, it appears that the proposed failure scenario is reasonable and that tanks free of primary cracking are likely free of secondary cracks. However, due to severe local deformations pressurization likely induces some level of local damage within fastener holes.

Reference

1. ASTM E 08-00, “Standard Test Methods for Tension Testing of Metallic Materials,” Annual Book of ASTM Standards, Section 8, Vol. 3.01.

2. ASTM E 399-00, “Standard Test Method for Plane-Strain Fracture Toughness of Metallic Materials,” Annual Book of ASTM Standards, Section 8, Vol. 3.01.

3. ASTM E 1820-00, “Standard Test Method for Measurement of Fracture Toughness,” Annual Book of ASTM Standards, Section 8, Vol. 3.01.

4. O’Brien, T.K., Murri, G.B., Hagemeier, R.J., and Rogers, C., “Combined Tension and Bending Testing of Tapered Composite Laminates,” Applied Composite Materials, Vol. 1, pp. 401-413, 1995.

5. James, M., and Swenson, D., "FRANC2D/L: A Crack Propagation Simulator for Plane Layered Structures," available from http://www.mne.ksu.edu/~franc2d/.

Appendix

Local Stress State Analysis

The initial attempts to design a specimen to reproduce the crack damage observed during pressurization failed, presumably because the specimens were overly simplified and were loaded differently (overly simplified local loading state) than the actual integrally-stiffened tank structure. A finite element analysis of the local stress state was performed to provide some guidance for a third specimen design. The objective here is to design a specimen with the same local stress state as the pressurized tank, and with a similar local geometry.

Cracks were detected propagating from pin loaded holes in the internal web of an integral stiffener tank. The tank was loaded by internal pressure with the hoop stress component acting on the web. An internal stiffener is attached to the web with mechanical fasteners and pin loading of the web is believed to occur at an angle of 18°, as shown in Figure A-1. The ratio of pin loading to total load is unknown, but believed to be significant (40-60%). The cracks were believed to have initiated on the side of the hole closest to the free edge first (primary crack) and propagated to the free edge before the initiation of a crack on the opposite side of the hole (secondary crack). The secondary crack is believed to arrest before reaching the external tank wall.

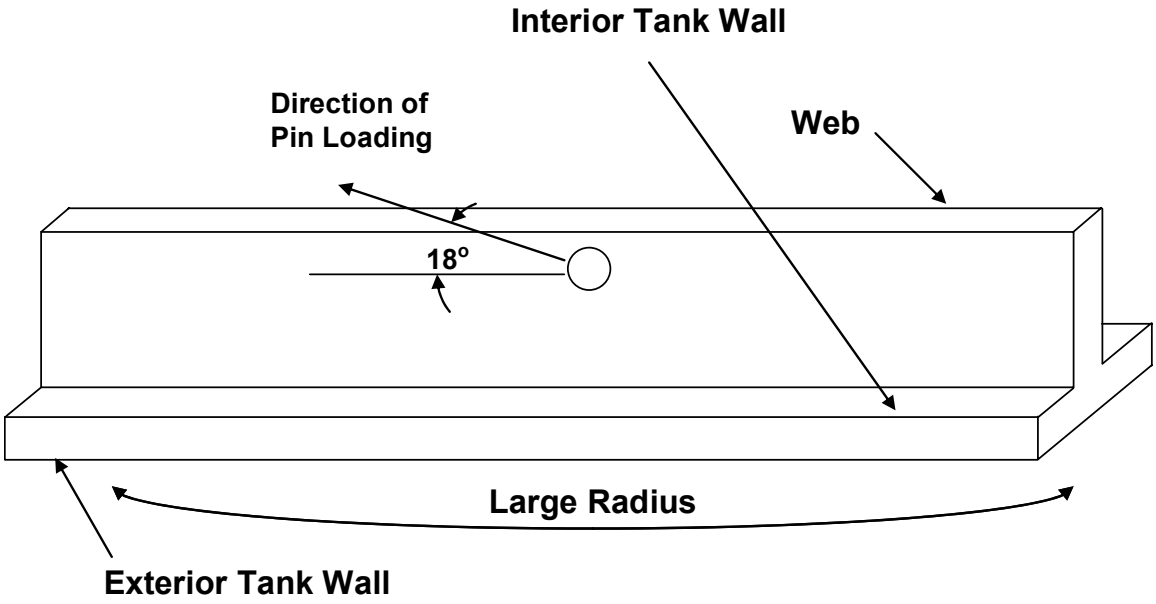

Figure A-1. Schematic of cracking location.

The goal of this study was to conduct elastic finite element analyses to assist in the design of test specimens for the assessment of the integral tank cracking problem. Three specimen designs were considered in the analysis: Single uniaxial with doublers, dual uniaxial, and T-bar biaxial, as shown schematically in Figures A-2, A-3, and A-4 respectively. The finite element code FRANC2DL (ref. 5) was used to perform the analyses. This code allowed the different components of the specimen (specimen, doublers, pins, etc.) to be represented by individual layers of elements with contact connections between layers. FRANC2DL is a two-dimensional finite element code, so any out-of-plane effects are ignored. An example finite element mesh is shown in Figure A-5. The analyses examined the ratio of the load transmitted in the doublers to the total applied load. An example of a stress contour plot is shown in Figure A-6.

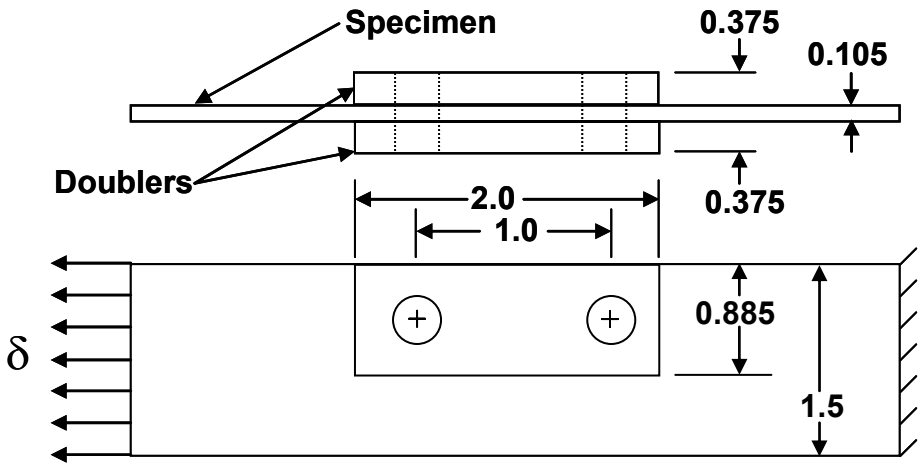

Figure A-2. Schematic of the single uniaxial specimen with doublers.

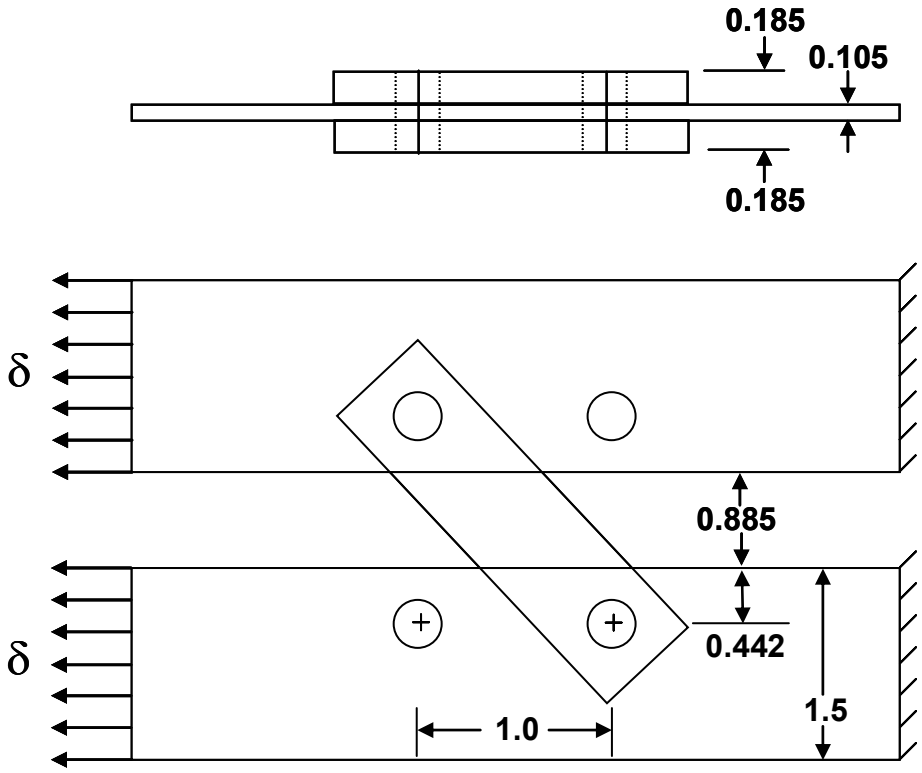

Figure A-3. Schematic of the dual uniaxial specimen with doublers.

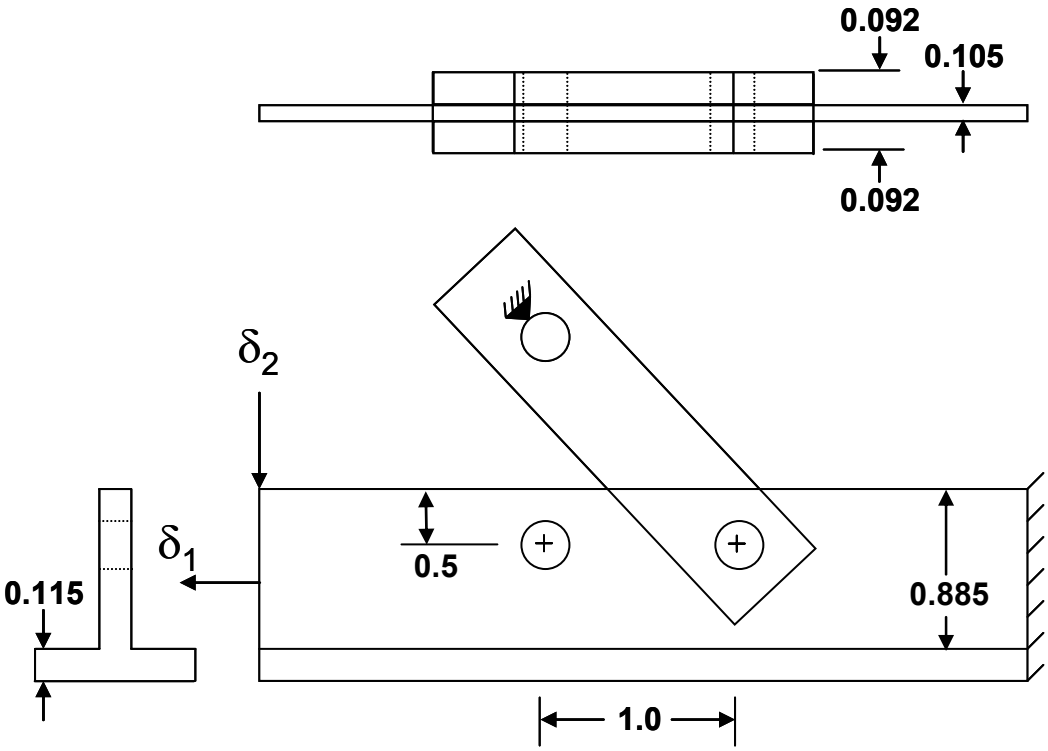

Figure A-4. Schematic of the biaxial T-bar specimen.

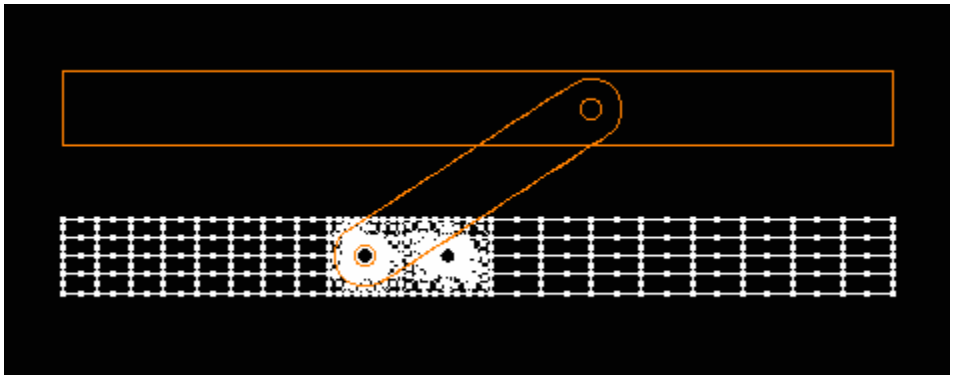

Figure A-5. Example of a finite element mesh for the dual uniaxial specimen with doublers.

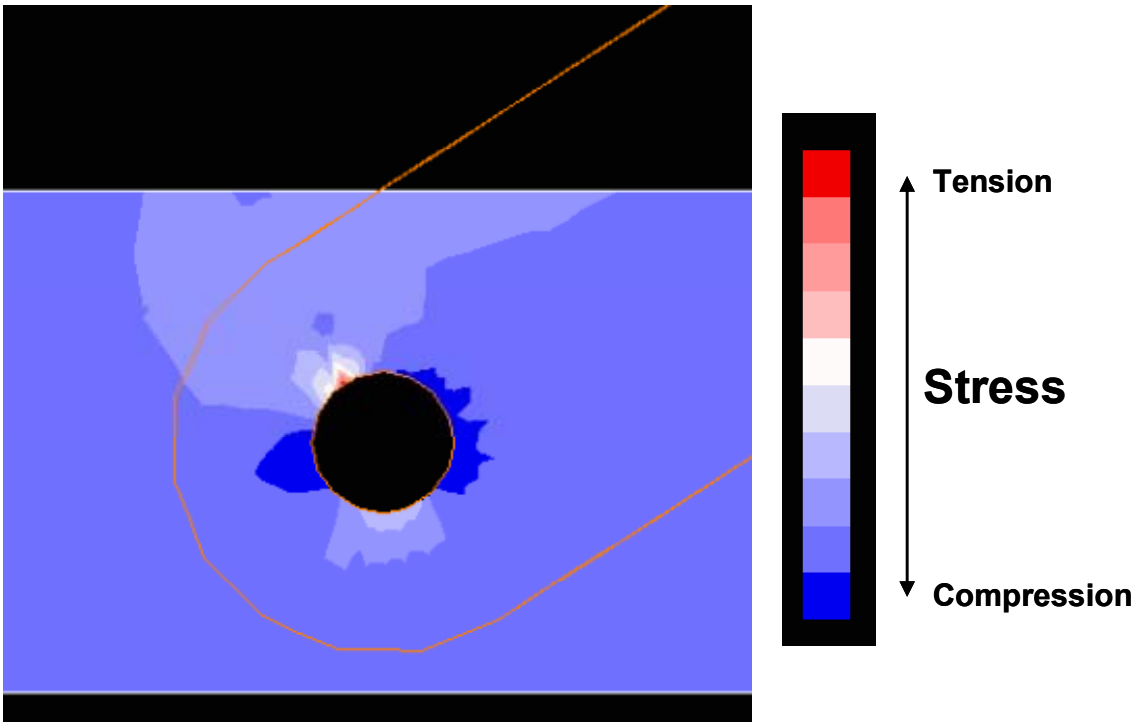

Figure A-6. Example of a stress contour plot for the dual uniaxial specimen with doublers.

The analysis for the single uniaxial specimen with doublers was performed by constraining the displacements along one end of the specimen and applying a uniform displacement (δ) to the opposite end, as shown in Figure A-2. The doublers were assumed to be attached to the specimen with snug fit pins. The modulus of the specimen and doublers was assumed to be 10,000 ksi and the modulus of the pins was assumed to be 30,000 ksi. The increased stiffness of the doublers will result in a portion of the load being transferred through the doublers, subjecting the holes to both pin loading and bypass loading.

The analysis for the dual uniaxial specimen was performed by creating two identical specimens, connecting holes in each of the specimens with doublers, and spacing the two specimens 0.885 inches apart, as shown in Figure A-3. The doublers were assumed to be attached to the specimen with snug fit pins. The modulus of the specimen was assumed to be 10,000 ksi and the moduli of the pins and doublers were assumed to be 30,000 ksi. The increased stiffness of the doublers will result in a portion of the load being transferred through the doublers, subjecting the connected holes to both pin loading and bypass loading. The pin loading will occur along the axis of the doublers, at an angle of about 30^{o} from the direction of loading.

The analysis of the T-bar biaxial specimen was performed by constraining the displacement and rotation of one end of the specimen, applying an axial displacement (δ_1) and an off-axis displacement (δ_2) to the other end of the specimen, and attaching doublers to one of the holes with a snug fit pin and constraining the other end of the doublers. The doublers resulted in a pin loading of one of the holes at about 20^{o} from the direction of the δ_1 displacement. The analysis was performed for several applied displacement ratios (δ_2/δ_1). The modulus of the specimen was assumed to be 10,000 ksi and the moduli of the pins and doublers were assumed to be 30,000 ksi; typical values for aluminum and steel, respectively.

Elastic analyses were conducted for two uniaxial specimens described above. The percentage of the load carried by the pin was determined for each analysis as shown in Table A-1. The pin load calculation determined the load carried by the doublers and divided by the total applied load.

Table A-1. Estimated ratio of pin load to total load.

Condition	Pin Load/Total Load
Single Uniaxial	0.12
Dual Uniaxial	0.19

The configuration of the T-bar biaxial specimen was considerably more complex due to both the variation in thickness of the specimen and the bending due to the off-axis loading. The load carried by the doublers can be calculated from the analysis, but a meaningful value of total load is difficult to define. The reaction forces at the displaced end of the T-bar specimen (R_{total}) and the reaction forces at the constrained end of the doublers ($R_{doubler}$) were used to estimate the extent of pin loading for several applied displacement ratios, as shown in Table A-2.

Table A-2. Estimated ratio of doubler reaction load to total reaction load.

δ_2/δ_1	$R_{doubler}/R_{total}$
0	0.26
1	0.43
2	0.57
5	0.83
10	1.06
20	1.24

The analysis was a simplified approach that allowed for the rapid assessment of several specimen design concepts, which enabled screening out designs that did not produce sufficient pin loading. The analysis did not account for plasticity at the hole, displacement of the pin, or loose fit pins, thus it provides an upper bound on the possible pin loading available for each specimen. Furthermore, the analysis did not model the biaxial loading fixture or exact location where the out-of-plane load was applied, both of which would decrease the amount of pin loading in the biaxial specimen.

REPORT DOCUMENTATION PAGE

Form Approved
OMB No. 0704-0188

1. REPORT DATE *(DD-MM-YYYY)*	2. REPORT TYPE	3. DATES COVERED *(From - To)*
01- 10 - 2008	Technical Memorandum	

4. TITLE AND SUBTITLE
Fracture Testing of Integral Stiffened Structure

5a. CONTRACT NUMBER

5b. GRANT NUMBER

5c. PROGRAM ELEMENT NUMBER

6. AUTHOR(S)
Newman, John A.; Smith, Stephen W.; Piascik, Robert S.; Dawicke, David S.; Johnston, William M.; and Willard, Scott A.

5d. PROJECT NUMBER

5e. TASK NUMBER

5f. WORK UNIT NUMBER
698259.02.07.07.03.03

7. PERFORMING ORGANIZATION NAME(S) AND ADDRESS(ES)
NASA Langley Research Center
Hampton, VA 23681-2199

8. PERFORMING ORGANIZATION REPORT NUMBER
L-19526

9. SPONSORING/MONITORING AGENCY NAME(S) AND ADDRESS(ES)
National Aeronautics and Space Administration
Washington, DC 20546-0001

10. SPONSOR/MONITOR'S ACRONYM(S)
NASA

11. SPONSOR/MONITOR'S REPORT NUMBER(S)
NASA/TM-2008-215530

12. DISTRIBUTION/AVAILABILITY STATEMENT
Unclassified - Unlimited
Subject Category 26
Availability: NASA CASI (301) 621-0390

13. SUPPLEMENTARY NOTES

14. ABSTRACT

Laboratory testing was conducted to evaluate safety concerns for integrally-stiffened tanks that were found to have developed cracks during pressurization testing. Cracks occurred at fastener holes where additional stiffeners were attached to the integrally-stiffened tank structure. Tests were conducted to obtain material properties and to reproduce the crack morphologies that were observed in service to help determine if the tanks are safe for operation. Reproducing the cracking modes observed during pressurization testing required a complex loading state involving both a tensile load in the integrally-stiffened structure and a pin-load at a fastener hole.

15. SUBJECT TERMS
Crack; Fracture; Integral-stiffened structure

16. SECURITY CLASSIFICATION OF:			17. LIMITATION OF ABSTRACT	18. NUMBER OF PAGES	19a. NAME OF RESPONSIBLE PERSON
a. REPORT	b. ABSTRACT	c. THIS PAGE			STI Help Desk (email: help@sti.nasa.gov)
					19b. TELEPHONE NUMBER *(Include area code)*
U	U	U	UU	32	(301) 621-0390